Approaching the Quantitative Description of Enantioselective Adsorption by Density Functional Theory Means

Francesc Viñes[†,*] and Oriol Lamiel-García[†]

[†]*Departament de Ciència de Materials i Química Física & Institut de Quimica Teòrica i Computacional (IQTCUB), Universitat de Barcelona, c/Martí i Franquès 1,08028 Barcelona, Spain.*

*corresponding author: francesc.vines@ub.edu

Abstract

The applications of enantiopure organic compounds range from medicine to green agrochemistry. Their racemic or enantioselective synthesis permits their acquisition beyond the extraction from life forms. These procedures need chiral resolution steps to achieve the required degrees of enantiomeric purity, though. Many research endeavours are addressed at finding chiral materials able to separate the enantiomers by their selective adsorption upon. Transition metal chiral surfaces have been found to reach enantiomeric excess degrees of purity outperforming surfaces of naturally existing chiral materials. Future research can be driven by high-throughput computational screening, given the employed methodology is able to discern the subtle enantiomeric differences of free energies of adsorption. The capabilities of density functional theory methods are here evaluated on the textbook case of *D*/*L*-aspartic acid adsorption on chiral $Cu(3,1,17)^{R\&S}$ metal surfaces. Results show that dispersive forces are a prerequisite to properly describe the enantioselective adsorption, whereas the inclusion of fundamental vibrational energy and adsorbate vibrational free energies are key ingredients to approach a quantitative description. Simulated X-ray photoemission and infrared spectra indicate that the adsorption conformations can be qualitatively recognized.

1

1. Introduction

The existence of pure enantiomers is crucial in life forms, from amino acids conforming enzymes to cell membrane or other metabolic proteins, which are, almost exclusively, present in their levorotatory (*L*) enantiomeric form. Furthermore, deoxyribonucleic acid (*DNA*) helixes are given in only one mirror image, due to their conformation based exclusively on the dextrorotatory (*D*) *D*-2-deoxyribose. Even sugars are exclusively metabolized on the *D*-form. Because of this, homochirality is considered a hallmark of life on Earth,[1] being of paramount importance when dealing with pharmaceuticals, where, very often, only one enantiomeric form of a compound is the essential active ingredient in a medicine.[2] This prompted the so-called *chiral switch* in pharmacy, but has spread over other fields, including *green* agrochemistry by enantiopure pesticides,[3] insect plague control in agriculture,[4] and even food and fragrance industries.[5,6]

Given these important fields of application, there are great worldwide research efforts aimed at obtaining enantiopure compounds, typically isolated from life form feedstocks. There have been large advances in the asymmetric synthesis by homogeneous catalysis, inferring chirality to common chemicals by chiral inducers, prochiral reactants, and/or chiral organometallic catalysts.[7-9] This asymmetric synthesis, either enantiospecific or racemic, requires further steps to separate the enantiomeric compounds from the reaction medium and the employed catalyst, as well as for the enantiospecific separation, so as to reach the sought degrees of purity. The enantioselectivity success is quantified according to the enantiomeric excess (*ee*), and most commonly achieved by high-performance chromatographic and electromigrating techniques using pure chiral selector solid phases.[10]

Research has been devoted at finding naturally chiral solid surfaces of minerals for such chiral resolution steps, although they typically display *ee* values of 1-2%, 10% at most,[11] with higher performances achieved by organic crystals chiral surfaces.[12] One particularly

appealing field of research is oriented at using chiral surfaces of catalytically active materials, in the quest of finding materials able carry out the enantioselective asymmetric synthesis by heterogeneous catalysis, thus benefitting from easier separation steps and a facile regeneration and recycling of the catalyst. However, another large share of research is focused on the solid-state separation of racemic mixtures of enantiomers, either isolated form life sources or non-enantiospecifically synthesized. A paramount work was achieved by Yun and Gellman, who showed that naturally chiral metal surfaces can yield *ee* values much higher than mineral surfaces, as demonstrated for Cu(3,1,17)$^{R\&S}$ surfaces, displaying an enantioselective adsorption of *D/L*-aspartic acid with an *ee* of $39 \pm 3\%$.[13] A later study revealed that such *ee* of a gas stream could be auto-amplified even on an achiral surface by a molecular preferential enantiospecific aggregation, as shown for *D/L*-aspartic acid on Cu(111).[14]

Despite there have been examples in the literature concerning enantioselective adsorption,[15] even reaction on chiral metal surfaces,[16] the still nowadays challenge is to unfold the origins of the enantioselective chemical adsorption, hampered by the difficulty of distinguishing two adsorbed enantiomers, due sometimes to the tiny differences of the Gibbs free energies of adsorption for both enantiomers. Experimentally, this has been achieved using radioisotopes of a given enantiomer,[13,17] although the procedure is costly and cumbersome. Indeed, this is an aspect where *ab initio* simulations on materials surface models could easily high-throughput screen a large number of situations, in order to determine the very nature of enantioselectivity, even to select possible candidates for maximizing the *ee*. There exist landmark examples of such detailed studies, typically employing Density Functional Theory (*DFT*),[18] although here the challenge is to be able to accurately quantify the subtle differences of a few hundreds of eV in the Gibbs free adsorption energies of the different enantiomers.

For instance, one can take *L*-alanine as a reference case, where DFT simulations have appointed the preferential adsorption of *L*-alanine on Cu(3,1,17)^S over *D*-Alanine by 0.03 eV/cell —2.89 kJ mol^{-1}/cell— at a moderate coverage,[19] as obtained using the Perdew-Wang (*PW91*) exchange-correlation functional.[20] A later study showed an amplified preferential adsorption at a full coverage adlayer situation of enantiopure phases of *L,L*-alanine on Cu(3,1,17)^S over the racemic *D,L*-alanine on Cu(3,1,17)^S situation by 0.091 eV/cell —8.78 kJ mol^{-1}/cell; note here that the *L,L*- notation implies enantiopure surface phases composed of *L*-enantiomer, and *D,L*- racemic phases composed of co-adsorbed *D*- and *L*- enantiomers. However, isotopically labelled *L*-alanine adsorption revealed a racemate surface phase with no measurable enantiospecificity.[21] This discrepancy could only be met with DFT simulations using the Perdew-Burke-Ernzerhof (*PBE*) exchange-correlation functional[22] —an exchange-correlation functional similar to PW91— accounting for dispersive forces through the Grimme D2 approximation,[23] revealing that the adlayer racemic phase is 0.01 eV/cell —0.96 kJ mol^{-1}/cell— more stable than the enantiopure *L,L*-alanine phase, and by that, underlining the key role played by dispersive forces, biasing this non-enantiospecific, racemic adsorption.

The open question mark is whether such DFT simulations accounting for dispersive forces are at a stage of accurately quantifying the small differences of free energies of adsorption as found in the literature. Thus, at variance with the *D,L*-alanine racemic adsorption case, here we address the enantiospecific adsorption of *D/L*-aspartic acid on Cu(3,1,17)$^{R\&S}$, assessing first whether DFT is able to reproduce the experimentally observed enantiomeric preferential adsorption, and, secondly, to determine the simulations accuracy in sizing the distinct free energies of adsorption, $\Delta\Delta G_{ads}$, measured of being 3.15 ± 0.29 kJ mol^{-1}.[13] The experimentally observed preference was found for *D*-aspartic acid over *L*-aspartic acid on Cu(3,1,17)^S, and could be detected by first saturating the Cu(3,1,17)^S chiral surface with isotopically labelled L-aspartic acid, *L-Asp, at 400 K. Later, the system was exposed D-

aspartic, *D*-Asp, at 460 K, which displaced the adsorbed *L-Asp until reaching an equilibrium between the adsorbed and gas phases. The kinetics of replacement allowed the authors stating the molecular adsorption and the adsorption preference of *D*-aspartic acid over *L*-aspartic acid on $Cu(3,1,17)^{S}$.[13]

In the present computational study attention is paid to other aspects possibly affecting the enantiospecific adsorption as discussed in the literature, such as the role of the molecular side chains,[24] the intact molecular adsorption of *D/L*-aspartic acid[13] compared to the deprotonated *D/L*-alanine adsorption[21] on $Cu(3,1,17)^{R\&S}$, or to the doubly deprotonated adsorption[25] of *D/L*-aspartic acid on $Cu(643)^{R\&S}$, the structure-sensitive enantiospecific adsorption,[26] the two-point *versus* three-point adsorption modes,[27] and newer aspects such as the fundamental vibrational energy effect, and the adsorbate free energy of vibration. The distinction of both enantiomers by quantitative and semi-quantitative surface science means is here tackled, thus going farther from the employed Scanning Tunnelling Microscopy (*STM*)[18] characterization, or the Temperature Programmed Reaction (*TPR*) and Desorption (*TPD*) spectroscopic analyses distinction,[13,26] here addressing a multitechnique point of view considering quantitative X-ray Photoemission Spectroscopy (*XPS*) and semi-quantitative infrared (*IR*) simulated spectra.

2. Computational Details

The DFT optimizations have been carried out within the Generalized Gradient Approximation (*GGA*), specifically, using the PBE functional,[22] known to be one of the most accurate in describing, in average terms, transition metal bulks and surface properties,[28,29] and normally a work horse functional for the adsorption of enantiomeric molecules on transition metal surfaces.[21] Following previous successful works,[21] dispersive forces were described through the Grimme D2 correction.[23] The Vienna *Ab initio* Simulation Package (*VASP*) suite, exploiting periodic boundary conditions, has been used for this purpose,[30] employing a plane-

wave basis set with a kinetic energy cutoff of 415 eV for the valence electron density, which delivers converged energy results with variations below 0.01 eV —0.96 kJ mol^{-1}/cell—, according to tests with increased kinetic cutoff energies. This reduced energy change is stressed throughout the study so as to define the limits of numerical accuracy of the presently DFT simulations.

The atomic core electron density has been described by the Projector Augmented Wave (*PAW*) method.[31] The optimizations have been carried out with an electronic convergence criterion of $1 \cdot 10^{-6}$ eV, and stopped when forces acting on the relaxed atoms were all below 0.01 eV Å^{-1}. All calculations were carried out in a non spin-polarized fashion, although spin-polarization tests revealed no surface magnetization, neither for the pristine Cu(3,1,17)^S surface, nor for the vacuum or adsorbed *D/L*-aspartic acid. A first order Methfessel-Paxton smearing was applied during optimizations, with an energy window of 0.2 eV, although final energies were extrapolated to the 0 K case with no smearing.

The Cu(3,1,17)^S vicinal chiral metal surface slab model has been constructed from the bulk Cu PBE optimized structure, self-consistently obtained, and available in the literature.[29] This slab contains 6 layers, where the three bottom ones have been kept frozen at bulk truncated positions, whereas the uppermost three layers were fully allowed to relax —*i.e.* 3+3 approach, see Figure 1, whereas more details of the pristine surface unit cell are displayed in the Figure S1 of the Supporting Information (*SI*). The adsorption of *L*- and *D*-aspartic acid enantiomers has been evaluated solely on Cu(3,1,17)^S chiral surface, as just inverse adsorption strengths are acquired on the Cu(3,1,17)^R surface —this is, a given adsorption mode of *D*-aspartic acid on Cu(3,1,17)^S is equivalent to the same mode of *L*-aspartic acid on Cu(3,1,17)^R by specular symmetry, and *vice versa*. This is confirmed by explicit simulations on the same conformation on the specular situation, acquiring consistently the same energies, although for the inverse chiral surface and enantiomer. A 5×3×1 Monkhorst-Pack **k**-point

mesh[32] has been used in the employed cell, with test calculations using a denser mesh revealing variations in total energy below 0.01 eV. 15 Å of vacuum were enough to isolate the periodically repeated slabs and to place the D/L-aspartic molecules inside, with variations in total energy below 0.01 eV using larger vacuum regions. During the optimizations, a counterdipole was added in the vacuum region so as to avoid dipole moment coupling between periodically repeated slabs along the surface direction.

The adsorption of a single molecule of either L-aspartic acid or D-aspartic acid on the $Cu(3,1,17)^S$ surface slab cell model has been systematically tackled assuming a three-point contact of the chiral molecules. The four substituents of the C chiral centre of aspartic acid are $-H$, $-NH_2$, $-COOH$, and $-CH_2COOH$. Thus, for each L- or D- enantiomer, the adsorption is contemplated with one of the chiral substituents pointing towards the vacuum, and the other three oriented at three regions of the $Cu(13,1,17)^S$ chiral surface, these are, the two asymmetric edges of the kinked step, having three (**3**) or (**2**) Cu atoms in length, see Figure 1, plus the (001) terraces. The rotation along the upwards substituent bond axis by 120° offers three different adsorption conformations per upward substituent. Note as well that the adsorption is considered here distinguishing the two sides of the kinked step, this is, considering two options for the (001) terrace, namely with a molecular chiral C substituent facing the lower-terrace (**LT**) or the upper-terrace (**UT**). Altogether, the total number of sampled conformations is 24 per enantiomer.

The site notation used here is different from the n_A_x notation defined previously by Rankin and Sholl,[33] and is adapted to the aforementioned sampling analysis. In detail, is defined as D/L-R^1-S^1-R^2-S^2-R^3-S^3, where considered R^1-R^3 are the substituents of the chiral C atom of the aspartic acid ($-H$, $-NH_2$, $-COOH$, or $-CH_2COOH$) in contact with the $Cu(3,1,17)^S$ chiral surface sites S^1-S^3 (**2** and **3**, combined with either **LT** or **UT**, see Figure 1). The fourth substituent is always considered pointing towards the vacuum region. Merely by this, the

enantiomers and adsorption modes are already unequivocally defined, although for clarity the *L* and *D* tags are added defining whether the *L*- or *D*-aspartic acid enantiomer is considered. See in Figure 2 the initial example of the *D*-NH$_2$-**2**-COOH-**3**-CH$_2$COOH-**UT** case.

The adsorption energy of *D/L*-aspartic acid on the Cu(3,1,17)^S chiral surface, E_{ads}, is defined as

$$E_{ads} = E_{(D/L)-Asp/Cu(3,1,17)^S} - E_{L-Asp} - E_{Cu(3,1,17)^S} \tag{1},$$

where the isolated *L*-aspartic acid energy, E_{L-Asp}, was calculated Γ-point placed in an asymmetric cell of 12×13×14 Å dimensions, ensuring 10 Å of vacuum in between periodically repeated cells and variations below 0.01 eV when using larger cells. Note that the same reference is used for *D*-aspartic acid adsorption as $E_{D-Asp} = E_{L-Asp}$, as explained above. The $E_{Cu(3,1,17)^S}$ energy term was obtained form the pristine, relaxed copper vicinal surface cell, whereas $E_{(D/L)-Asp/Cu(3,1,17)^S}$ is the energy of the relaxed system containing a *D*- or *L*-aspartic acid molecule adsorbed on the Cu(3,1,17)^S slab surface model. Within this definition, the more negative the adsorption energy, the stronger the adsorption is.

The adsorption energies can be corrected accounting for the Zero Point Energy (*ZPE*), added to the gas phase or adsorbed molecule energies, and defined as

$$ZPE = \sum_i^{NMV} \frac{1}{2} h v_i \tag{2},$$

where the *i* index goes over the total number of Normal Modes of Vibration (*NMV*), each one with its characteristic vibrational frequency v_i, being *h* the Planck constant. The NMV are 3N-6 for the gas phase molecule, being N the number of atoms of the molecule, and thus discounting the three rotational and three translational modes. However, NMV is 3N for the adsorbed molecules, as there the free molecular rotations and translations become frustrated when adsorbed, and effectively converted into vibrations. The vibrational frequencies for the gas phase and adsorbed molecules have been acquired within the harmonic approximation *via*

finite displacements method of 0.03 Å in length, thus building and diagonalizing the Hessian matrix, and neglecting the coupling with the substrate phonon vibrations for the adsorbed molecule cases.

3. Results and Discussion

3.1. Enantioselective Adsorption

The obtained adsorption energies, either gained from PBE or PBE-D2 optimizations, are listed in Table 1. Notice that some values are not reported, belonging to cases where the adsorption lead to a molecular disaggregation, not observed in the experiments,[13] or to a weak adsorption conformation (physisorption), also not detected in the experiments.[13] In this last sense, conformations with a difference in adsorption energy with respect the most stable situation higher than 100 kJ mol^{-1} have been disregarded. The results in Table 1 show enantiomeric preferences, in accordance to experiments,[13] but, when considering PBE results, the preference is for L-aspartic acid instead of the experimentally observed D- preference.[13] Explicitly, the most stable situation is the L-H-**2**-NH$_2$-**3**-COOH-**LT** case, while the closest situation in energetic stability preference for D-aspartic acid is the D-COOH-**2**-H-**3**-CH$_2$COOH-**LT**, with a difference in adsorption energies, ΔE_{ads}, of 22.82 kJ mol^{-1}/cell. This energetic stability preference is well beyond the above-commented present numerical accuracy of ~0.98 kJ mol^{-1}/cell, and also beyond the DFT accuracy of ~10 kJ mol^{-1}. Therefore, the results do not seem to be computationally or theoretically biased, allowing its later discussion.

Figure 3 shows the adsorbed geometries of these most stable situations for each enantiomer, and several quite important aspects can be withdrawn. First of all, the kinked step ledge seems to be the main anchoring point for both L- and D-aspartic acid situations, in accordance with the known fact that the metallic activity increases when the atomic

coordination number drops.[34,35] The observed minima imply a two-point coordination of a single chiral C substituent, not following the three-point contact model, usually accepted for chiral recognition.[36] Even though there are reported cases of two-point contact chiral resolutions,[27] the present PBE situations imply a one point contact, going against the lock and key mechanism. However, the enantioselective adsorption may be explained based on other intra- and intermolecular interactions, see discussion in the SI.

This full picture completely changes, though, when considering PBE-D2 optimized structures. First of all, the accounting of dispersive forces leads to generally flatter adsorption conformations, see Figure 4, at variance to the PBE more upright adsorption, see Figure 3. Such flat-lying structures resemble those of D/L-cysteine on Au(17,1,19)^S, although there these were obtained using the Revised PBE ($RPBE$) functional, and, therefore, without implicitly accounting for a description of dispersive forces.[27] Here the planarity is fundamentally different in its origin, since, at variance with the aforementioned case, the more planar adsorption conformations results from a maximization of van der Waals types of interaction with respect to the Cu(3,1,17)^S surface, overcoming a higher electronic repulsion responsible of the PBE upright conformations.

Furthermore, most importantly, and related to the previous, is that the enantiomeric preference is reversed, indeed targeting the experimental observations.[13] Based on PBE-D2 optimized geometries and energies, the strongest adsorption is for D-aspartic acid on Cu(3,1,17)^S, resulting from sampling the D-COOH-**2**-CH$_2$COOH-**3**-NH$_2$-**UT** site, and is preferred over the strongest adsorption of L-aspartic acid on the L-H-**2**-COOH-**3**-CH$_2$COOH-**LT** site by 12.28 kJ mol^{-1}/cell. Apparently, as happened on the racemic adsorption of D,L-alanine on Cu(3,1,17)^{S},[24] the dispersive forces inclusion seems to be a critical, determining factor necessary for the duly forecast of enantioselective or racemic enantiomeric adsorptions.

A closer inspection of the adsorbed L- and D-enantiomers reveal that they display a very resembling flat structure, with similar intramolecular H···O bonds between –CH$_2$COOH and –COOH groups of 1.680 and 1.798 Å lengths, respectively. The major differences relate with their position with respect to the Cu(3,1,17)^S vicinal surface. In the case of L-aspartic acid, the –COOH and –NH$_2$ groups seem to contact the **3** and **2** sites, or, namely, the step ledge and kink sites, respectively. Aside, the –CH$_2$COOH lies over the **LT** site. This three-point conformation differs from the initial departing L-H-**2**-COOH-**3**-CH$_2$COOH-**LT** structure, and, actually, in the course of the optimization, the –H and –NH$_2$ groups rotated. That implied –H being pointed towards the Cu(3,1,17)^S substrate, but, as the molecule spreads over the **LT**, there is still room to accommodate it without compromising the conformational energy, see Figure 4.

In the case of the D-aspartic acid, the enantiomer is quite located over the kinked step region, on the **UT** side. Actually, the interaction is as strong as to slightly bend the molecular framework, allowing the interaction of –CH$_2$COOH, -COOH, and –NH$_2$ groups with the **2**, **3**, and step ledge positions, respectively. As happened with L-aspartic acid enantiomer, the final three-point contact adsorption differs from the initially sampled D-COOH-**2**-CH$_2$COOH-**3**-NH$_2$-**UT** position, here involving a lateral displacement and a rotation of the molecule along the –H group axis. Although not apparently critical, it is worth highlighting that there exist intermolecular hydrogen bonds on both L- and D-aspartic acid enantiomers, as found also for other amino acids adsorbed on chiral metal surfaces.[37] In the L-aspartic acid case, there are two, one O···H in between –COOH and –CH$_2$COOH groups of vicinal molecules, and another H···N in between –COOH and –NH$_2$ groups as well, with 2.015 and 1.712 Å lengths, respectively. In the case of D-aspartic acid, there is only one H···N hydrogen bond in between –COOH and –NH$_2$ groups, with a bond length of 1.865 Å, see Figure S3 in the SI.

11

A further aspect to consider is whether the distinct adsorption energies for the *L*- and *D*-aspartic enantiomers are affected by the ZPE or the experimental conditions, and to what extent. Table 2 gathers the above-commented ΔE_{ads} values neglecting (PBE) or accounting for dispersive forces (PBE-D2). The addition of the fundamental vibrational energy (ZPE) on the latter is minor, of 2.58 kJ mol⁻¹/cell, although by that ZPE helping at bringing together simulations and experimental results, with a *D*-aspartic acid adsorption energy preference over *L*-aspartic acid on Cu(3,1,17)^S chiral surface being 9.70 kJ mol⁻¹/cell, thus closer to the experimental reported value of 3.15 ± 0.29 kJ mol⁻¹.[13]

However, the commented experimental reference is based on differences of Gibbs free energies of adsorption, $\Delta\Delta G_{ads}$, obtained at an equilibration temperature of 460 K, and averaged over different flux ratios of gas phase *D*- and *L*-aspartic acid mixtures.[13] Here, $\Delta\Delta G_{ads}$ has been approximated based on the *Ab Initio* Thermodynamics (*AIT*) approach.[38] A careful analysis of the energetic contributions revealed that, for a racemic flux ratio where partial pressures of *L*- and *D*-aspartic acid are equal, the only difference on Gibbs free energies of adsorption for *L*- and *D*-aspartic acid raises from the different vibrational free energies of the adsorbates, G^{vib}, where

$$G^{vib} = \sum_{i=1}^{NMV} k_B T ln \left(1 - exp \left(\frac{h v_i}{k_B T} \right) \right) \qquad (3),$$

applicable for already ZPE-corrected energies. The addition of this vibrational free energy on the PBE-D2 ZPE results, at a working temperature of 460 K, yields a $\Delta\Delta G_{ads}$ value of 2.12 kJ mol⁻¹/cell, surprisingly almost matching the experimental mean value of 3.15 ± 0.29 kJ mol⁻¹, specially when one considers the current calculations numerical accuracy of 0.98 kJ mol⁻¹/cell. Despite of this apparent excellent agreement, one has to be cautious on stating that PBE-D2 simulations accounting for ZPE and G^{vib} are able to quantitatively evaluate $\Delta\Delta G_{ads}$, as such difference may still be affected by the DFT methodology inherent accuracy. However,

12

it seems clear that such DFT simulations can at least qualitatively determine the enantioselective adsorption of chiral molecules on chiral metal surfaces. Furthermore, it seems clear as well that vibrational aspects of the adsorbed enantiomers, these are, the ZPE correction and the vibrational free energy, are key at trying to quantitatively determine the $\Delta\Delta G_{ads}$, and, ultimately, the *ee* performance of the metal chiral surface.

3.2. Recognition by Surface Science Techniques

As a last point, the possible distinction of both *D*/*L*-aspartic acid enantiomers on the Cu(3,1,17)$^{R\&S}$ chiral surfaces is analysed well beyond the previously employed STM imaging,[18] as regularly applied on other species in the past, or the TPD or TPR mediated differentiation of the adsorption strengths.[13] Here we evaluated the quantitative XPS or Photoemission Electron Spectroscopy (PES) detection of such adsorbates, being an extended procedure to characterize and quantify adsorbates in surface science.[39] The Binding Energies (*BE*) of C, N, and O 1*s* aspartic acid core levels have been firstly evaluated on the PBE and PBE-D2 optimized structures, being BE obtained at the Initial State (*IS*) approximation, thus, neglecting core level relaxation energies,[40] or, from another perspective, assuming that the relaxation magnitudes for the distinct atoms of the same type are comparable. Notice that, even though such IS BEs are severely underestimated compared to the experimental values, their relative positions, ΔBEs, follow the experimental trends, as demonstrated on an extensive study of 185 1*s* BEs of 68 organic molecules.[41]

The obtained PBE-D2 results are presented in Figure 5 as a Gaussian functions convolution of 0.5 eV of Full Width at Half Maximum (*FWHM*), while PBE results are shown in Figure S4 of the SI. On Figure S4 one sees that the PBE upright conformations imply four distinguishable C atoms (**a-d**), but the similitudes in between *L*- and *D*-enantiomers would prevent their sole unequivocal identification. The same seems to apply to O 1*s* signals (**e-h**), where there would be two overlapped signals in the middle spectrum

region. Only N 1s would permit discerning in between the adsorbed L- and D-aspartic acid enantiomer, being their shift in between BEs (ΔBEs) of ~0.5 eV.

However, when dealing with the likely flat adsorption conformations of D/L-aspartic acid as obtained from PBE-D2 optimizations, the situation changes, see Figure 5. In principle, for both enantiomers, the C 1s spectra would have three signals instead of four, with the two highest BE peaks overlapped. The matching between enantiomers is also found for the N 1s levels. Finally, for O 1s BEs, one would observe two overlapped signals for both enantiomers, but not that different in between themselves so as to allow their distinction. Notice that the relative positions of the four C (**a-d**) and O (**e-h**) change from one enantiomer to the other for both PBE and PBE-D2 situations. Figure S5 of the SI shows the 1s BEs for the PBE-D2 geometries, but without the Cu(3,1,17)^{S} chiral surface substrate. The complete neglecting of the substrate electron density on the aspartic acid BEs remedies the different ordering, and therefore, highlights the underlying effect of the chiral metal surface on the particular D/L-aspartic acid BEs and their ordering.

In summary, the use of XPS or PES techniques would permit certifying the flat adsorption of aspartic acid *versus* the upright, given the number and intensity of C and O 1s signals, although the distinction of enantiomers appears to be a challenging task, possible, if any, only when using High Resolution XPS (HR-XPS) or PES (HR-PES), as there the accuracy can reach 0.1 eV limits for BEs and ΔBEs.[39]

The simulated IR spectra, shown in Figure 6, further evidence the different characterization of upright (PBE) and flat-like (PBE-D2) adsorption conformations, in the sense that in the former cases, the more perpendicular orientation of the D- and L- adsorbed enantiomers fosters high-intensity signals, in line to the surface selection rule applied to the changes of the molecular dipole moment component perpendicular to the surface along the molecular vibration. However, the intensities decay by an order of magnitude when having

flat conformations, as observed resulting form PBE-D2 optimizations. Within these considerations, the IR spectra are complex involving 48 vibrations, and further discussion is based merely on those, highest-intensity peaks. These belong to C-O stretching modes for PBE simulated IR, but of the –COOH substituent in the case of *L*-aspartic acid, with a vibrational frequency of 1638 cm^{-1}, whereas for the *D*-aspartic acid the maximum peak is blue-shifted by 116 cm^{-1} to a final value of 1754 cm^{-1}, belonging to the C-O stretching of the –CH$_2$COOH substituent.

Nevertheless, the most IR active peaks on flat, PBE-D2 geometries, are found in the 2600-2800 cm^{-1} range, a region IR-transparent to the just commented upright PBE geometries, thus, directly allowing characterizing flat conformations of *D/L*-aspartic acid enantiomers. Further than that, the most intense signal for *L*-aspartic acid is the C-H stretching of the chiral C atom (**a**), located at 2632 cm^{-1}, which would be completely distinguishable from the most intense peak for *D*-aspartic acid, being blue-shifted by 110 cm^{-1} to a final number of 2742 cm^{-1}, and belonging to the O-H stretching of the –COOH substituent. Both IR stretching signals are quite related to the quite perpendicular display of such bonds with respect the Cu(3,1,17)^S chiral surface. Summarizing, the appearance of signals in the 2600-2800 cm^{-1} region would be indicative of the flat adsorption of *D/L*-aspartic acid enantiomers, and the relative location would imply the presence of *D*- or *L*- enantiomers, although the semi-quantitative nature of IR spectra would allow only qualitative statements on their surface population.

4. Conclusions

Here the capabilities of modern DFT methods in describing enantioselective adsorption processes are put at stakes, with the ultimate aim of determining whether they are suitable for qualitative or quantitative predictions of enantiomeric resolution on chiral metal surfaces. To this end, the enantioselective adsorption of *D/L*-aspartic acid on chiral Cu(3,1,17)$^{R\&S}$ metal

surface is taken as an exemplary textbook case, whose enantiomer difference in Gibbs free energy of adsorption, $\Delta\Delta G_{ads}$, is known to be of 3.15 ± 0.29 kJ mol^{-1}.[13]

The systematic adsorption of *D*- and *L*-aspartic acid enantiomers, carried out on a Cu(3,1,17)^S slab model, was performed using the PBE functional, but also including a dispersive forces description (PBE-D2). The results reveal that PBE unduly describes a preference of adsorption of *L*- over *D*-aspartic acid enantiomer by 22.82 kJ mol^{-1}/cell, with upright conformers that only accomplish the three-point contact rule of chiral recognition when accounting for inter- and intramolecular distinct interactions. The inclusion of dispersive forces (PBE-D2) seems to be a requirement to remedy such a situation, thus properly describing a preference of adsorption for *D*-Aspartic acid by 12.28 kJ mol^{-1}/cell and three-point contact structures with respect the Cu(13,1,17)^S surface, with flatter adsorption conformations found for both enantiomers.

The inclusion of vibrational energy contributions, through ZPE and vibrational free energies of the adsorbates, allows reducing the discrepancy with respect the experimental measurements, with an $\Delta\Delta G_{ads}$ estimated value at 460 K and equal partial pressures of both enantiomers of 2.12 kJ mol^{-1}/cell, thus, revealing that vibrational contributions are non-negligible, key aspects to be regarded when aiming at the quantitative determination of the enantioselective adsorption on metal chiral surfaces in particular, yet likely to apply as well on other types of chiral surfaces.

The possible recognition and quantification of the different adsorbed enantiomers of aspartic acid is addressed under the scope of XPS measurements, by estimations of aspartic acid C, N, and O 1*s* BEs. However, the simulated XPS spectra seem only to offer the possibility in distinguishing upright (PBE) from flat (PBE-D2) adsorption conformations, unless HR-XPS could be applied with ΔBEs accuracies in the order of 0.1 eV. The simulation of IR spectra reveal complex fingerprints, which possibly could only serve to semi-

quantitatively discern in between both adsorbed enantiomers with flat adsorption conformations (PBE-D2), displaying highest intensity signals in the 2600-2800 cm^{-1} region, where *L*- and *D*- enantiomers signals are spaced by 110 cm^{-1}, allowing its discrete characterization.

Notes

Acknowledgements

Table 1. Sampled adsorption sites for *L*- and *D*-aspartic acid on Cu(3,1,17)^S chiral metal surface, along with their site locations, and the adsorption energy difference with respect the most stable structure, ΔE_{ads}, as obtained both at PBE and PBE-D2 levels.

	2	3	LT	UT	ΔE_{ads} PBE kJ mol^{-1}	ΔE_{ads} PBE-D2 kJ mol^{-1}
L-	CH$_2$COOH	NH$_2$	H	—	—	—
	COOH	NH$_2$	CH$_2$COOH	—	—	—
	H	**NH$_2$**	**COOH**	—	**0.00**	26.40
	CH$_2$COOH	COOH	NH$_2$	—	52.13	54.04
	H	**COOH**	**CH$_2$COOH**	—	36.97	**12.28**
	NH$_2$	COOH	H	—	38.28	17.97
	NH$_2$	H	CH$_2$COOH	—	29.22	13.96
	CH$_2$COOH	H	COOH	—	24.62	12.70
	COOH	H	NH$_2$	—	60.73	66.38
	H	CH$_2$COOH	NH$_2$	—	6.62	13.89
	NH$_2$	CH$_2$COOH	COOH	—	—	—
	COOH	CH$_2$COOH	H	—	50.22	21.09
	CH$_2$COOH	NH$_2$	—	H	58.69	72.40
	COOH	NH$_2$	—	CH$_2$COOH	62.10	69.84
	H	NH$_2$	—	COOH	66.24	82.20
	CH$_2$COOH	COOH	—	NH$_2$	77.75	97.04
	H	COOH	—	CH$_2$COOH	64.97	70.95
	NH$_2$	COOH	—	H	51.35	62.21
	NH$_2$	H	—	CH$_2$COOH	83.73	28.77
	CH$_2$COOH	H	—	COOH	64.85	71.97
	COOH	H	—	NH$_2$	83.74	42.36
	H	CH$_2$COOH	—	NH$_2$	77.39	97.73
	NH$_2$	CH$_2$COOH	—	COOH	65.30	72.11
	COOH	CH$_2$COOH	—	H	42.22	29.14
	CH$_2$COOH	NH$_2$	—	NH$_2$	58.69	72.40
	COOH	NH$_2$	—	CH$_2$COOH	62.10	69.84
	H	NH$_2$	—	H	66.24	82.20
D-	H	NH$_2$	CH$_2$COOH	—	34.05	42.51
	CH$_2$COOH	NH$_2$	COOH	—	34.03	42.47
	COOH	NH$_2$	H	—	—	—
	NH$_2$	COOH	CH$_2$COOH	—	30.82	28.32
	CH$_2$COOH	COOH	H	—	—	37.45
	H	COOH	NH$_2$	—	62.87	46.93
	CH$_2$COOH	H	NH$_2$	—	34.03	42.42

|					
COOH	**H**	**CH₂COOH**	—	**22.82**	—
NH₂	H	COOH	—	60.70	—
NH₂	CH₂COOH	H	—	35.12	18.92
COOH	CH₂COOH	NH₂	—	37.38	36.94
H	CH₂COOH	COOH	—	73.32	61.10
H	NH₂	—	CH₂COOH	87.49	92.21
CH₂COOH	NH₂	—	COOH	—	88.83
COOH	NH₂	—	H	87.58	92.77
NH₂	COOH	—	CH₂COOH	73.25	32.36
CH₂COOH	COOH	—	H	—	—
H	COOH	—	NH₂	63.02	3.35
CH₂COOH	H	—	NH₂	68.14	76.38
COOH	H	—	CH₂COOH	—	—
NH₂	H	—	COOH	74.68	34.05
NH₂	CH₂COOH	—	H	65.67	45.07
COOH	**CH₂COOH**	—	**NH₂**		**0.00**
H	CH₂COOH	—	COOH	65.67	72.85

Table 2. Adsorption energy differences, ΔE_{ads}, with respect the most stable structure adsorption sites for L- and D-aspartic acid on Cu(3,1,17)^S chiral metal surface, as obtained either from PBE or PBE-D2 simulations, as well as that of PBE-D2 ZPE-corrected. The difference of Gibbs free energy of adsorption, $\Delta\Delta G_{ads}$, is also estimated upon PBE-D2 ZPE results at assuming a racemic mixture of L- and D-aspartic acid gas phase partial pressures, and an equilibration temperature of 460 K.

| | ΔE_{ads} | | | $\Delta\Delta G_{ads}$ |
| | PBE | PBE-D2 | PBE-D2 ZPE | PBE-D2 ZPE |
Aspartic acid	**kJ mol^{-1}**	**kJ mol^{-1}**	**kJ mol^{-1}**	**kJ mol^{-1}**
L-	0.00	12.28	9.70	2.12
D-	22.82	0.00	0.00	0.00

Figure 1. Eagle-eye view of the employed Cu(3,1,17)^S supercell, where the chirality is defined by the three-point rotation marked with the green arrow. Note that Cu(3,1,17)^R surface would the specular image to the one here shown. Cu atoms are denoted as pale pink spheres, although those Cu atoms located at the kinked steps are shown as bright pink spheres to guide the eyes. The explored adsorption positions around the asymmetrically kinked steps are defined by the space within three reference regions, including the three-atom edge (**3**), the two-atom edge (**2**), and either the lower terrace (**LT**) or the upper terrace (**UT**) (001) surfaces.
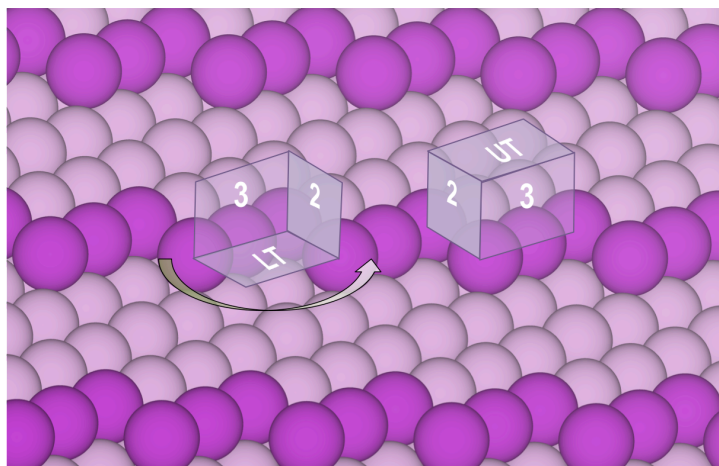
Figure 2. Top view of the D-NH$_2$-**2**-COOH-**3**-CH$_2$COOH-**UT** adsorption model of D-aspartic acid on the employed Cu(3,1,17)^S supercell. Carbon, Nitrogen, Oxygen, and Hydrogen atoms are shown as light blue, brown, red, and pale white spheres, respectively. The rest of the coloured atoms are as in Figure 1.
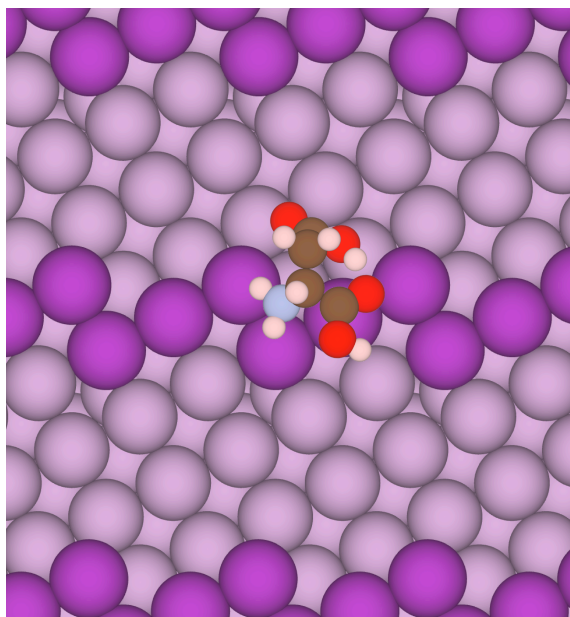
Figure 3. Top (left panels) and side (right panels) views of most stable adsorption sites of *L*-(top panels) and *D*-aspartic acid (bottom panels), as obtained from PBE optimizations. Colour coding as in Figure 2.
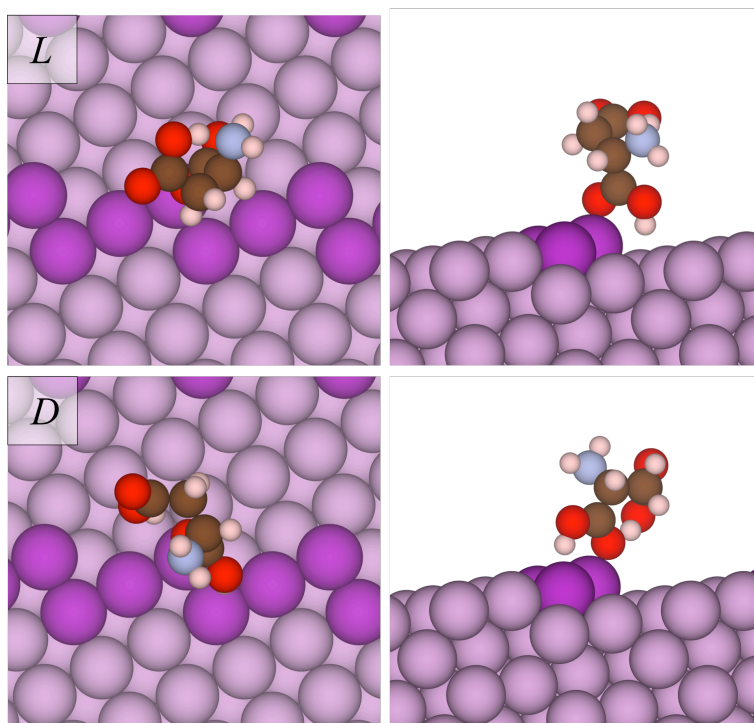
Figure 4. Top (left panels) and side (right panels) views of most stable adsorption sites of *L*-(top panels) and *D*-aspartic acid (bottom panels), as obtained from PBE-D2 optimizations. Colour coding as in Figure 2.
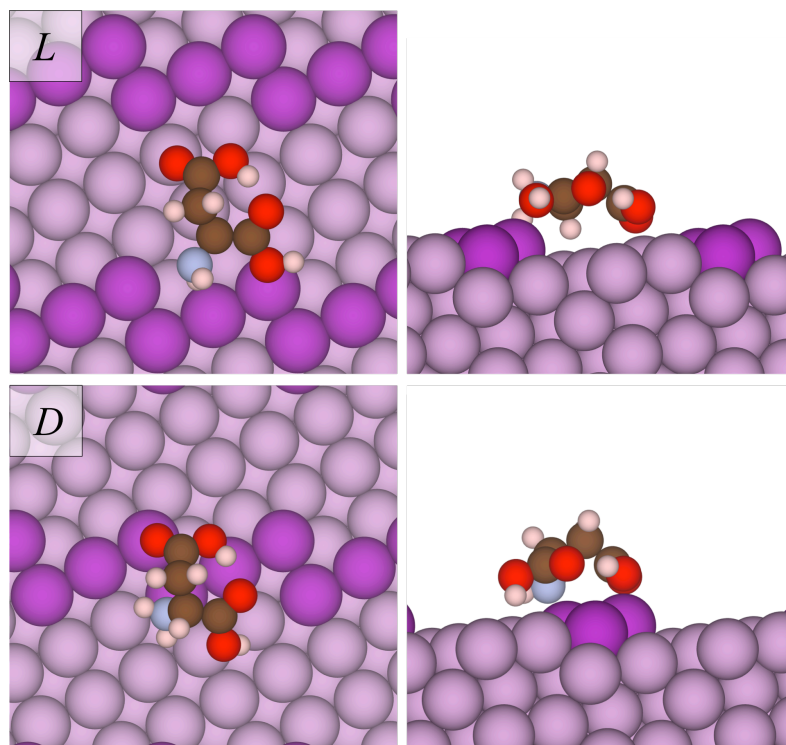
Figure 5. Gaussian convoluted 1s core level BEs, obtained within the IS approximation, of C, N, and O atoms of most stable adsorption conformations of L- and D-aspartic acid on Cu(3,1,17)^S chiral surface, as obtained from PBE-D2 optimizations. Molecular inset specifies, for L-aspartic acid, the distinct C (**a-d**) or O (**e-h**) atoms. Atomic spheres colour code follows that of Figure 2.
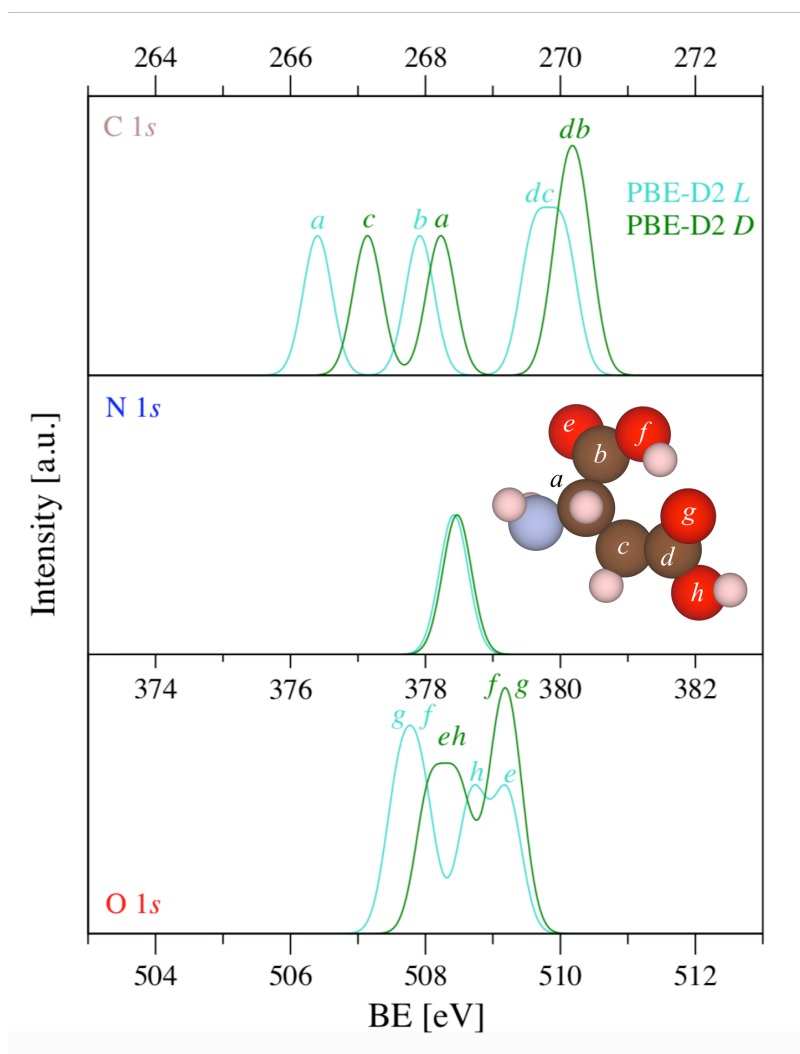
Figure 6. Simulated IR for most stable adsorption conformations of *L*- and *D*-aspartic acid on Cu(3,1,17)^S chiral surface, as obtained from either PBE or PBE-D2 optimizations. The intensity of the peaks of the PBE-D2 situation has been magnified ten times for visualizations purposes.
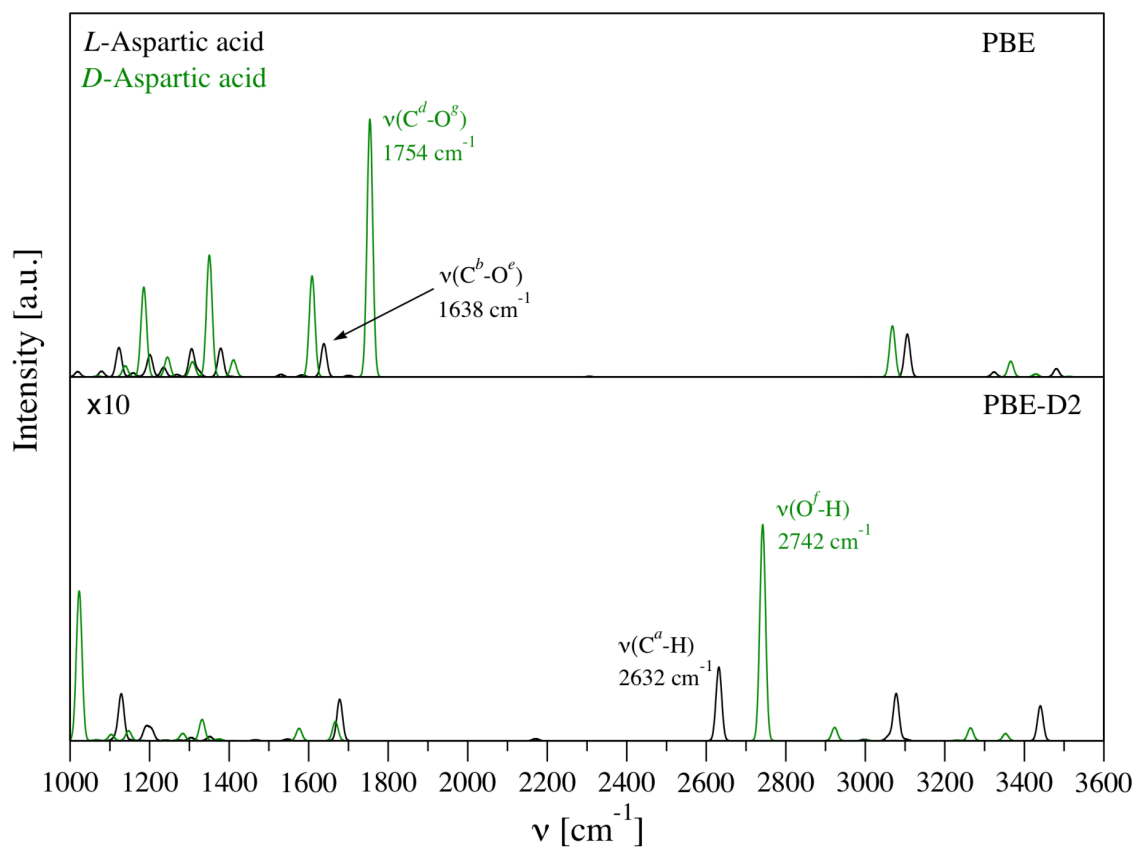
References

(1) Bonner, W. A.; Kavasmaneck, P. R.; Martin, F. S.; Flores, J. J. Asymmetric Adsorption by Quartz: A Model for the Prebiotic Origin of Optical Activity. *Origins Life* **1975**, *6*, 367-376.

(2) Adam, S. S.; Breesloff, P.; Mason, C. G. Pharmacological Differences between the Optical Isomers of Ibuprofen: Evidence for Metabolic Inversion of the (-)-Isomer. *J. Pharm. Pharmacol.* **1976**, *28*, 256-257.

(3) López, O.; Fernández-Bolanos, J. G.; Gil, M. V. New Trends in Pest Control: The Search for Greener Insecticides. *Green Chem.* **2005**, *7*, 431-442.

(4) Mori, K. Significance of Chirality in Pheromone Science. *Bioorg. Med. Chem.* **2007**, *15*, 7505-7523.

(5) Shallenberger, R. S. *Taste Chemistry*, 1st Edition, Glasgow, Blakie Academic & Professional (1993).

(6) Leitereg, T. J.; Guadagni, D. G.; Harris, J.; Mon, T. R.; Teranishi, R. Evidence for the Difference between the Odours of the Optical Isomers (+)- and (−)-Carvone. *Nature* **1971**, *230*, 455-456.

(7) Noyori, R. Asymmetric Catalysis: Science and Opportunities. *Angew. Chem. Int. Ed.* **2002**, *41*, 2008-2022.

(8) Knowles, W. S. Asymmetric Hydrogenations. *Angew. Chem. Int. Ed.* **2002**, *41*, 1998-2007.

(9) Sharpless, K. B. Searching for New Reactivity. *Angew. Chem. Int. Ed.* **2002**, *41*, 2024-2032.

(10) Chankvetadze, B. Enantioseparations by Using Capillary Electrophoretic Techniques. The Story of 20 and a Few More Years. *J. Chromatogr. A* **2007**, *1168*, 45-70.

(11) Hazen, R. M.; Filley, T. R.; Goodfriend, G. A. Selective Adsorption of L- and D-Amino Acids on Calcite: Implications for Biochemical Homochirality. *Proc. Natl. Acad. Sci.* **2001**, *98*, 5487-5490.

(12) Weissbuch, I.; Leiserowitz, L.; Lahav, M. Achiral Organic, Inorganic, and Metal Crystals as Auxiliaries for Asymmetric Transformations. *Isr. J. Chem.* **2011**, *51*, 1017-1033.

(13) Yun, Y.; Gellman, A. J. Enantioselective Separation on Naturally Chiral Metal Surfaces: *D,L*-Aspartic Acid on Cu(3,1,17)$^{R\&S}$ Surfaces. *Angew. Chem. Int. Ed.* **2013**, *52*, 3394-3397.

(14) Yun, Y.; Gellman, A. J. Adsorption-Induced Auto-Amplification of Enantiomeric Excess on an Achiral Surface. *Nat. Chem.* **2015**, *7*, 520-525.

(15) Horvath, J. D.; Koritnik, A.; Kamakoti, P.; Sholl, D. S.; Gellman, A. J. Enantioselective Separation on a Naturally Chiral Surface. *J. Am. Chem. Soc.* **2004**, *126*, 14988-14994.

(16) Attard, G. A. Electrochemical Studies of Enantioselectivity at Chiral Metal Surfaces. *J. Phys. Chem. B* **2001**, *105*, 3158-3167.

(17) Bonner, W. A.; Kavasmaneck, P. R.; Martin, F. S.; Flores, J. J. Asymmetric Adsorption of Alanine by Quartz. *Science* **1974**, *186*, 143-144.

(18) Humblot, V.; Haq, S.; Muryn, C.; Hofer, W. A.; Raval, R. From Local Adsorption Stresses to Chiral Surfaces: (*R,R*)-Tartaric Acid on Ni(110). *J. Am. Chem. Soc.* **2002**, *124*, 503-510.

(19) Rankin, R. B.; Sholl, D. S. First-Principles Studies of Chiral Step Reconstructions of Cu(100) by Adsorbed Glycine and Alanine. *J. Chem. Phys.* **2006**, *124*, 074703.

(20) Perdew, J. P.; Chevary, J. A.; Vosko, S. H.; Jackson, K. A.; Pederson, M. R.; Singh, D. J.; Fiolhais, C. Atoms, Molecules, Solids, and Surfaces: Applications of the Generalized Gradient Approximation for Exchange and Correlation. *Phys. Rev. B* **1992**, *46*, 6671-6687.

(21) Yun, Y.; Wei, D.; Sholl, D. S.; Gellman, A. J. Equilibrium Adsorption of *D*- and *L*-Alanine Mixtures on Naturally Chiral Cu$\{3,1,17\}^{R\&S}$ Surfaces. *J. Phys. Chem. C* **2014**, *118*, 14957-14966.

(22) Perdew, J. P.; Burke, K.; Ernzerhof, M. Generalized Gradient Approximation Made Simple. *Phys. Rev. Lett.* **1996**, *77*, 3865-3868.

(23) Grimme, S. Semiempirical GGA-Type Density Functional Constructed with a Long-Range Dispersion Correction. *J. Comput. Chem.* **2006**, *27*, 1787-1799.

(24) Yun, Y.; Gellman, A. J. Enantiospecific Adsorption of Amino Acids on Naturally Chiral Cu$\{3,1,17\}^{R\&S}$ Surfaces. *Langmuir* **2015**, *31*, 6055-6063.

(25) Mhatre, B. S.; Dutta, S.; Reinicker, A.; Karagoz, B.; Gellman, A. J. Explosive Enantiospecific Decomposition of Aspartic Acid on Cu Surfaces. *Chem. Commun.* **2016**, *52*, 14125-14128.

(26) Gellman, A. J.; Huang, Y.; Koritnik, A. J.; Horvath, J. D. Structure-Sensitive Enantiospecific Adsorption on Naturally Chiral Cu(*hkl*)$^{R\&S}$ Surfaces. *J. Phys.: Condens. Matter* **2017**, *29*, 034001.

(27) Greber, T.; Šljivancanin, Ž.; Schillinger, R.; Wider, J.; Hammer, B. Chiral Recognition of Organic Molecules by Atomic Kinks on Surfaces. *Phys. Rev. Lett.* **2006**, *96*, 056103.

(28) Vega, L.; Ruvireta, J.; Viñes, F.; Illas, F. Jacob's Ladder as Sketched by Escher: Assessing the Performance of Broadly Used Density Functionals on Transition Metal Surface Properties. *J. Chem. Theory Comput.* **2018**, 14, 395-403.

(29) Janthon, P.; Luo, S.; Kozlov, S.M.; Viñes, F.; Limtrakul, J.; Truhlar, D.G.; Illas, F. Bulk Properties of Transition Metals: A Challenge for the Design of Universal Density Functionals. *J. Chem. Theory Comput.* **2014**, 10, 3832-3839.

(30) Kresse, G.; Furthmüller, J. Efficient Iterative Schemes for Ab Initio Total-Energy Calculations Using a Plane-Wave Basis Set. *Phys. Rev. B* **1996**, *54*, 11169-11186.

(31) Blöchl, P. E. Projector Augmented-Wave Method. *Phys. Rev. B* **1994**, 50, 17953-17979.

(32) Monkhorst, H. J.; Pack, J. D. Special Points for Brillouin-Zone Integrations. *Phys. Rev. B* **1976**, *13*, 5188-5192.

(33) Rankin, R.; Sholl, D. Structures of Dense Glycine and Alanine Adlayers on Chiral Cu(3,1,17) Surfaces. *Langmuir* **2006**, *22*, 8096-8103.

(34) Mavrikakis, M.; Stoltze, P.; Nørskov, J. K. Making Gold Less Noble. *Catal. Lett.* **2000**, 64, 101-106.

(35) Calle-Vallejo, F.; Loffreda, D.; Koper, M. T. M.; Sautet, P. Introducing Structural Sensitivity into Adsorption–Energy Scaling Relations by Means of Coordination Numbers. *Nat. Chem.* **2015**, *7*, 403-410.

(36) Easson L. H.; Stedman, E. Studies on the Relationship between Chemical Constitution and Physiological Action. *Biochem. J.* **1933**, *27*, 1257-1266.

(37) Fajín, J. L. C.; Gomes, J. R. B.; Cordeiro, M. N. D. S. DFT Study of the Adsorption of *D*-(*L*-)Cysteine on Flat and Chiral Stepped Gold Surfaces. *Langmuir* **2013**, *29*, 8856–8864.

(38) Rogal, J.; Reuter, K. *Ab Initio Atomistic Thermodynamics for Surfaces: A Primer*, in *Experiment, Modeling and Simulation* of Gas-Surface Interactions for Reactive Flows in Hypersonic Flights, Educational Notes RTO-EN-AVT-142, Neuilly-sur-Seine, France (2007).

(39) Papp, C.; Steinrück, H.-P. In Situ High-Resolution X-Ray Photoelectron Spectroscopy – Fundamental Insights in Surface Reactions. *Surf. Sci. Rep.* **2013**, *68*, 446-487.

(40) Viñes, F.; Sousa, C.; Illas, F. On the Prediction of Core Level Binding Energies in Molecules, Surfaces and Solids. *Phys. Chem. Chem. Phys.* **2018**, *20*, 8403-8410.

(41) Pueyo-Bellafont, N.; Viñes, F.; Hieringer, W.; Illas, F. Predicting Core Level Binding Energies Shifts: Suitability of the Projector Augmented Wave Approach as Implemented in VASP. *J. Comput. Chem.* **2017**, *38*, 518-522.

TOC Graphic

DFT + vdW + ZPE + G^{vib} ≈ $\Delta\Delta G_{ads}$

Exp.

racemic

D/*L*-Asp

Cu(13,1,17)^S